



ELSEVIER

Available online at [www.sciencedirect.com](http://www.sciencedirect.com)

ScienceDirect

journal homepage: [www.intl.elsevierhealth.com/journals/dema](http://www.intl.elsevierhealth.com/journals/dema)

# High strength polymer/silicon nitride composites for dental restorations

Feng Wang<sup>a,b</sup>, Jingshu Guo<sup>a</sup>, Ke Li<sup>a</sup>, Jian Sun<sup>c,\*</sup>, Yuping Zeng<sup>a</sup>,  
Congqin Ning<sup>a,\*</sup>

<sup>a</sup> State Key Laboratory of High Performance Ceramics and Superfine Microstructure, Shanghai Institute of Ceramics, Chinese Academy of Sciences, Shanghai, 200050, China

<sup>b</sup> NTNU Nanomechanical Lab, Department of Structural Engineering, Norwegian University of Science and Technology (NTNU), Trondheim, 7491, Norway

<sup>c</sup> Department of Prosthodontics, Ninth Peoples Hospital, School of Medicine, Shanghai Jiao Tong University, Shanghai, 200011, China

## ARTICLE INFO

### Article history:

Received 15 January 2019

Received in revised form

19 May 2019

Accepted 22 May 2019

### Keywords:

Porous Si<sub>3</sub>N<sub>4</sub>

Polymer-infiltrated Si<sub>3</sub>N<sub>4</sub>  
composites

Dental restoration

Cytocompatibility

## ABSTRACT

**Objectives.** To fabricate polymer-infiltrated silicon nitride composite (PISNC) and evaluate the potential of PISNC in dental application.

**Methods.** Porous silicon nitride (Si<sub>3</sub>N<sub>4</sub>) ceramics were fabricated through gelcasting and pressureless sintering. Polymer infiltrating was carried out then and composites were obtained after curing of polymer. Flexural strength and microstructures of porous ceramic scaffolds and polymer-infiltrated composites were obtained by three-point bending and SEM, respectively. Phase distributions of polymer-infiltrated ceramics were observed by EDS. Human gingival fibroblast cells (HGFs) were used to evaluate the cytocompatibility and IL-6 release. The cell morphology were observed by SEM. The amount of released IL-6 was investigated using ELISA test system.

**Results.** Porosity and mechanical strength of porous ceramics ranged from 45.1 to 49.3% and 171.8–262.3 MPa, respectively. The bicontinuous structure of polymer-infiltrated composites possessed them with excellent mechanical properties. Porosity and mechanical strength of polymer-infiltrated Si<sub>3</sub>N<sub>4</sub> composites ranged from 1.94 to 2.28% and 273–385.3 MPa, respectively. Additionally, the PISNC enhanced the initial adhesion and spreading activity of HGFs compared with PMMA. The PISNC showed similar IL-6 release performance with PMMA samples.

**Significances.** The PISNC is a promising candidate for dental restorations and high-load medical applications.

© 2019 The Academy of Dental Materials. Published by Elsevier Inc. All rights reserved.

\* Corresponding authors.

E-mail addresses: [doctorsunjian74@aliyun.com](mailto:doctorsunjian74@aliyun.com) (J. Sun), [cqning@mail.sic.ac.cn](mailto:cqning@mail.sic.ac.cn) (C. Ning).

<https://doi.org/10.1016/j.dental.2019.05.022>

0109-5641/© 2019 The Academy of Dental Materials. Published by Elsevier Inc. All rights reserved.

## 1. Introduction

Silicon nitride ( $\text{Si}_3\text{N}_4$ ) ceramics possess excellent properties such as high strength, hardness, wear resistance and thermal shock resistance [1–3], which lead to wide applications of  $\text{Si}_3\text{N}_4$  ceramics as bearings, heat engine components, cutting tools, hot gas filters, radome materials, and so on [3–5]. Recently, silicon nitride ( $\text{Si}_3\text{N}_4$ ) based ceramics have attracted more and more attention in biomedical fields due to their inherent bioinert characteristic and good biocompatibility. The possibility of using silicon nitride ceramics for structural orthopaedic implants has been well explored and proved by Mazzocchi et al. [6,7]. And diamond-like carbon (DLC) modified  $\text{Si}_3\text{N}_4$  ceramics has been proved to be well adequate for articular prostheses medical application [8]. Badran et al. also suggest  $\text{Si}_3\text{N}_4$  implants as a promising choice in dental implantology [9]. However, all-ceramic restoration of  $\text{Si}_3\text{N}_4$  ceramics may result in excessive wear of opposing teeth. Ceramic-polymer composite strategy is considered as an effective way to improve the comprehensive performance of all-ceramic restorations.

Composites of polymer and ceramic are expected to combine advantages of both components. Comparing with mono-phase polymers or ceramics, polymer-ceramic composites are likely to achieve an elastic modulus similar to natural bone tissue. However, it seems that polymer-based composites always show low strength and low toughness, which restrict their wide applications. Generally, polymer-ceramic composites fabricated by dispersing ceramic particles in polymer matrixes can improve the strength of polymers to some extent [10,11]. While the mechanical properties of polymers limit the final mechanical properties of polymer-ceramic composites since the polymer phase provide a continuous network in this case. A new way that can effectively improve the mechanical properties of resin-ceramic composites has been reported recently. This method creates a bicontinuous network which contains a porous ceramic structure and an interpenetrated polymer phase [12,13]. The porous ceramic skeletons can provide the composites with high strength and moderate hardness. In this case, both inorganic and organic phases are continuous in the composites. Thus, the advantages of organic and inorganic part can be utilized to the most.

$\text{Si}_3\text{N}_4$  ceramic with elongated grains is supposed to be an excellent candidate of porous matrix. High strength porous  $\text{Si}_3\text{N}_4$  ceramics with moderate porosity can be obtained through gelcasting with IBMA (copolymer of isobutylene and maleic anhydride) and pressureless sintering [14]. By infiltrating polymer into high strength porous  $\text{Si}_3\text{N}_4$  skeletons, bicontinuous ceramic-polymer composites with excellent mechanical strength can be fabricated. Which can broaden the use of  $\text{Si}_3\text{N}_4$  ceramics in high load-bearing medical applications, especially in dental applications.

In present work, porous  $\text{Si}_3\text{N}_4$  scaffolds with various porosity were fabricated through gel casting method from suspensions with different solid content. Bicontinuous PISNCs were then fabricated by infiltrating PMMA resin into porous scaffolds followed by a polymerization process. Microstructure, mechanical performance of the porous ceramic matrix

and PISNCs were investigated. The cytocompatibility of PISNCs were also compared with PMMA and  $\text{Si}_3\text{N}_4$  ceramics.

## 2. Experimental procedure

### 2.1. Fabrication of polymer-infiltrated $\text{Si}_3\text{N}_4$ composites

Porous  $\text{Si}_3\text{N}_4$  ceramics were fabricated through gelcasting and liquid-phase sintering.  $\text{Si}_3\text{N}_4$  powder ( $\alpha$ -phase  $\geq 95$  wt%;  $d_{50} = 0.5 \mu\text{m}$ ; Ube Industries Ltd., Japan),  $\text{Y}_2\text{O}_3$  powder (5.0  $\mu\text{m}$ ; purity  $\geq 99.99$  wt%; Yuelong Company, Shanghai, China) and copolymer of isobutylene and maleic anhydride (IBMA, Isobam104#, Kuraray Co., Ltd., Osaka, Japan) were added into distilled water and milled with  $\text{Si}_3\text{N}_4$  balls for 2.5 h at a rotating speed of 350 r/min. Solid content of the suspensions were 50 wt%, 55 wt%, and 60 wt%. The obtained homogeneous slurries were casted into plastic molds and then consolidated. After demolding, the green bodies were dried at room temperature for 48 h. Finally, the samples were heated up to 600 °C in vacuum with a dwell time of 2 h to remove organic additives followed by sintering at 1700 °C for 2 h under  $\text{N}_2$  atmosphere to obtain porous  $\text{Si}_3\text{N}_4$  ceramics.

The as-received porous  $\text{Si}_3\text{N}_4$  ceramics were immersed into 3-(Trimethoxysilyl) propyl methacrylate (KH-570, Sinopharm Chemical Reagent Co., Ltd., Shanghai, China) solution (the solvent was ethanol) with a concentration of 5 wt% for 3 h followed by a drying at 120 °C. The silane-coupling agent treated samples were subsequently immersed in the monomer solution of Methyl methacrylate (MMA, Huliang Biological Technology Co., Ltd., Shanghai, China) containing 1 wt% benzoyl peroxide (BPO, Huliang Biological Technology Co., Ltd., Shanghai, China) for 24 h, followed by a polymerization procedure at 150 °C for 1 h under atmospheric pressure. Porous  $\text{Si}_3\text{N}_4$  ceramics obtained from suspensions with solid content of 50 wt%, 55 wt%, 60 wt% were named as SN50, SN55, SN60, respectively. Polymer-infiltrated  $\text{Si}_3\text{N}_4$  composites obtained from SN50, SN55, SN60 were named as PSN50, PSN55, PSN60, respectively.

Fig 1 illustrated the detailed procedure of polymer infiltrating in the present work. The elongated  $\text{Si}_3\text{N}_4$  grains stacked together and resulted in well connected pores in porous ceramic scaffolds. As immersing porous  $\text{Si}_3\text{N}_4$  scaffolds into PMMA resin, polymer monomers infiltrated into pores automatically due to the capillarity. After dwelling for certain time, pores in ceramic scaffolds were filled by polymer monomers. Then polymer infiltrated composites were fabricated by in-situ curing of PMMA.

### 2.2. Characterization of microstructure and mechanical properties

Morphologies of the samples were observed by scanning electron microscope (SEM, S-3400 N, Hitachi, Japan). The back scattered electron (BSE) and corresponding energy dispersive spectrometer (EDS) images of PISNCs were observed by a field-emission scanning electron microscope (FE-SEM, SU8220, Hitachi, Japan). Porosity of porous  $\text{Si}_3\text{N}_4$  ceramics and polymer-infiltrated  $\text{Si}_3\text{N}_4$  ceramics were measured

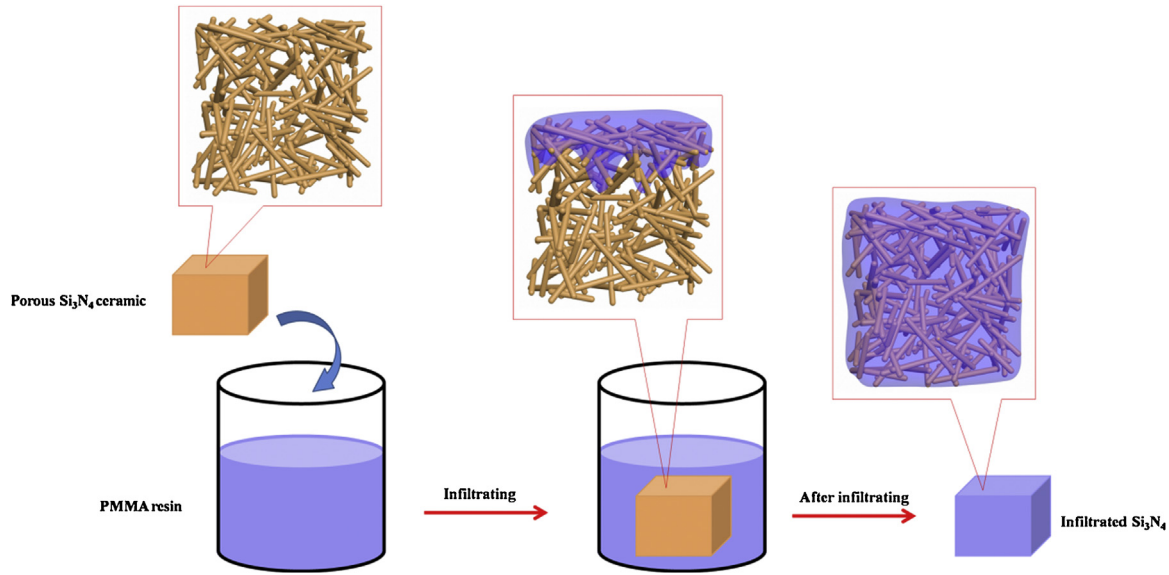


Fig. 1 – Schematic illustration of polymer infiltrating procedure.

by Archimedes method. Flexural strength were tested via a three-point bending method with a span of 30.0 mm and a cross-head speed of  $0.5 \text{ mm min}^{-1}$  using specimens with dimensions of  $3.0 \text{ mm} \times 4.0 \text{ mm} \times 36.0 \text{ mm}$  (Instron-5566, Instron Co., Ltd., American). The tensile surface was polished with diamond paste before testing. Five parallel samples of each composition were used for the measurements of flexural strength and open porosity. Micro-hardness measurements were carried out on a Vickers hardness tester (TUKON-2100B, Instron Co., Ltd., American) and the mean value was an average of five measurements.

## 2.3. Cytocompatibility

### 2.3.1. Sample treatment

PSN60 ceramic-polymer composite was selected as a representative polymer-infiltrated  $\text{Si}_3\text{N}_4$  composite to evaluate the cytocompatibility and cytokine release behavior, compared with pure PMMA and  $\text{Si}_3\text{N}_4$  samples. Surface of the samples were ground and polished to get a similar condition to clinical use. The polished samples were ultrasonically cleaned with ethonal, sterilized water and acetone in turn and then dried in air. Finally, all the samples were autoclaved at  $150^\circ\text{C}$  for 60 min.

### 2.3.2. Cell culture

Human gingival fibroblast cells (HGFs, Department of Orthopedics, Shanghai Sixth People's Hospital, Shanghai, China) were used to evaluate the cytocompatibility and IL-6 release. HGFs were cultured in a 5%  $\text{CO}_2$  incubator at  $37^\circ\text{C}$  with the d-minimum essential medium (D-MEM, Gibco, Invitrogen Inc.) containing 10% fetal bovine serum (FBS, Hyclone, USA) and 1% antimicrobial of penicillin and streptomycin (Hyclone, USA). Cell culture medium was changed every 2 days. Before reseeding cells on the sample surface, HGFs were detached from the  $75 \text{ cm}^2$  flasks with 1 ml trypsin/EDTA (0.25% trypsin, 0.02% EDTA) (Gibco, Invitrogen) at  $37^\circ\text{C}$  with 5%  $\text{CO}_2$  for one min-

utes followed by a centrifugation at 1000 rpm for 5 min. Then, the supernatant was removed and proper amount of DMEM was added to prepare cell suspensions with cell densities of  $10.0 \times 10^4$  cells/ml and  $5.0 \times 10^4$  cells/ml.

### 2.3.3. Cell morphology

The autoclaved samples were put in a 24-well culture plate and 1 mL HGFs suspension with a cell density of  $10.0 \times 10^4$  cells/ml were added to each sample. At each collecting time point, the samples with HGFs were transferred to a new 24-well plate and washed with phosphate buffered saline (PBS) for twice. Afterwards, an overnight fixation in 2.5% glutaraldehyde was performed. The fixed samples were then dehydrated in a graded series of ethanol solutions (30, 50, 75, 90, 95 and 100 v/v %) and then dried in air. The cell morphology were then observed by SEM.

### 2.3.4. Cell proliferation

$300 \mu\text{l}$  HGFs suspension with a cell density of  $5.0 \times 10^4$  cells/ml were added to each sample and cultured for 2d, 5d and 7d. At each collecting time point, the samples were transferred to a new 96-well plate, then  $150 \mu\text{l}$  D-MEM of 10 v/v% alamar blue was added to each sample and cultured for another 2 h. Afterwards,  $100 \mu\text{l}$  of the above medium was transferred into a 96-well black plate and the fluorescent intensity was measured with an excitation wavelength and emission wavelength of 560 nm and 590 nm, respectively.

### 2.3.5. Cytokine analysis

Samples were put into a 96-well culture plate.  $300 \mu\text{l}$  HGFs suspension with a cell density of  $10.0 \times 10^4$ /ml were added to each well and cultured for 6 h, 1d, and 2d. At each collecting time point, the supernatant was collected and fresh culture medium was added. All the collected supernatant was stored at  $-20^\circ\text{C}$  before testing. The amount of released IL-6 was investigated using ELISA test system according to the manufacturer's instructions (Human IL-6 Elisa Kit, Invitrogen,

USA). The amount of cytokine release was quantified against a standard curve of purified human IL-6.

#### 2.4. Statistical analysis

All data were expressed as mean  $\pm$  standard deviation (SD). The statistically significant difference was measured using two-way analysis of variance and Tukey's multiple comparison tests. Statistical analysis was carried out using a GraphPad Prism 5 software package and the value of  $p < 0.05$  was considered statistically significant.

### 3. Results

#### 3.1. Porosity and mechanical performance of porous $\text{Si}_3\text{N}_4$ ceramics and PISNCs

Open porosity and flexural strength of the porous  $\text{Si}_3\text{N}_4$  ceramics and PISNCs were shown in Fig. 2a–b. It could be seen that the porosity of  $\text{Si}_3\text{N}_4$  scaffolds decreased slightly with the increase in  $\text{Si}_3\text{N}_4$  content. Accordingly, the flexural strength showed an increase with the increase in  $\text{Si}_3\text{N}_4$  content. All porous  $\text{Si}_3\text{N}_4$  scaffolds possessed excellent mechanical strength with moderate porosity as expected. These high strength porous scaffolds guaranteed the excellent mechanical strength of PISNCs. After polymer infiltrating process, nearly fully dense composites (with porosity less than 2.3%) could be obtained and the flexural strength was greatly improved. The flexural strength of PSN60 reached up to 385.3 MPa. The hardness of PISNCs was less than 2.4 GPa and the elastic modulus is less than 59.3 MPa, which is similar to human bone tissues. It indicated that PISNCs possessed excellent flexural strength with moderate hardness and elastic modulus (Fig. 1c–d).

#### 3.2. Microtopography of porous $\text{Si}_3\text{N}_4$ scaffolds and PISNCs

Fig. 3 showed the fracture surface of porous  $\text{Si}_3\text{N}_4$  ceramic SN50 and its corresponding polymer-infiltrated composite PSN50. The micrographs revealed typical elongated  $\text{Si}_3\text{N}_4$  grains in porous  $\text{Si}_3\text{N}_4$  ceramic through liquid-phase-sintering mechanism [14]. After polymer was infiltrated, few pores were detected on the cross section of PSN50 sample, indicating a well infiltration of polymer and good combination of ceramic phase and polymer phase.

#### 3.3. Surface elemental characterization of PISNCs

Element analysis of PSN50 were shown in Fig. 4. The back scattered electron (BSE) image in Fig. 4a revealed the possible distribution of ceramics and polymer phase by the difference between brightness. In the Fig. 4a, the white flakes represented the location of yttrium (Y) which was the heaviest element among the existed elements in the sample. The darkest part represented the location of element carbon (C). Thus, the brighter parts showed area of element nitrogen (N). The energy dispersive spectrometer (EDS) results in Fig. 4b–d further confirmed the distribution of elements N, C and Y by

direct pointed out the distribution of them on the surface. The three elements could be regarded as references of  $\text{Si}_3\text{N}_4$ , PMMA and  $\text{Y}_2\text{O}_3$ , respectively. Thus the interpenetrated structure of ceramic skeleton and polymer were verified.

#### 3.4. Response of HGFs

To be successfully used in vivo, the cytocompatibility of PSN60 were evaluated using HGFs. Pure medical PMMA and  $\text{Si}_3\text{N}_4$  were used as controls. SEM morphologies of HGFs cultured on various surfaces at various time points were shown in Fig. 5. After 1 h culture, HGFs on PMMA surface exhibited a spherical morphology with few filopodia, while the cells seeded on  $\text{Si}_3\text{N}_4$  and PSN60 samples spread much faster than those on PMMA surface, both filopodia and lamellipodia could be clearly observed. With an increase of culture time, HGFs on  $\text{Si}_3\text{N}_4$  and PSN60 samples showed polygonal sharps with plenty of filopodia and lamellipodia while the cells on PMMA just started to spread. After 24 h culture, HGFs on all samples displayed a flat spreading with a lot of filopodia and lamellipodia. The cells on  $\text{Si}_3\text{N}_4$  and PSN60 samples displayed much better adhesion than those on PMMA. The above results indicated that PSN60 samples enhanced the initial adhesion and spreading activity of HGFs compared with PMMA.

The proliferation of HGFs cultured on sample surfaces were estimated by the alamar blue assay and the results were shown in Fig. 6. At the early stage of culture, there were no statistically difference among the three groups. After 5 and 7 days culture, the cell proliferation on  $\text{Si}_3\text{N}_4$  samples was slightly higher than that on PMMA and PSN60 samples, but the differences were not significant. In general, HGFs on all three samples showed a significantly increase with the increase in culture time, indicating PSN60 and the control groups were all favorable to the growth and proliferation of HGFs.

IL-6 was generally regarded as one of the key cytokines which were involved in the induction and regulation of host responses in the inflammatory reactions [15]. In order to determine the early gingival and periodontal inflammation caused by the three kinds of materials, the release of IL-6 from HGFs was investigated and the results were shown in Fig. 7. In a whole, the IL-6 released at very low level for all the groups at all collecting time points. At all the collecting time points,  $\text{Si}_3\text{N}_4$  sample showed a lower level of IL-6 release than PMMA and PSN60 samples, indicating  $\text{Si}_3\text{N}_4$  ceramic had a superior biocompatibility. While the IL-6 release was no significant difference between PSN60 and PMMA samples. Thus the composite PSN60 were potential to have comparable biocompatibility with medical PMMA.

### 4. Discussion

Gelcasting has always been proved as a way to fabricate ceramics with uniform microstructure and excellent mechanical performance since reported by Omatete et al. [16–18]. Generally, fabricating porous scaffolds with high strength were one of the most essential points to obtain polymer-infiltrated composites with excellent mechanical properties. Thus, porous  $\text{Si}_3\text{N}_4$  ceramics fabricated through gelcasting that possessed high strength were promising candidates of

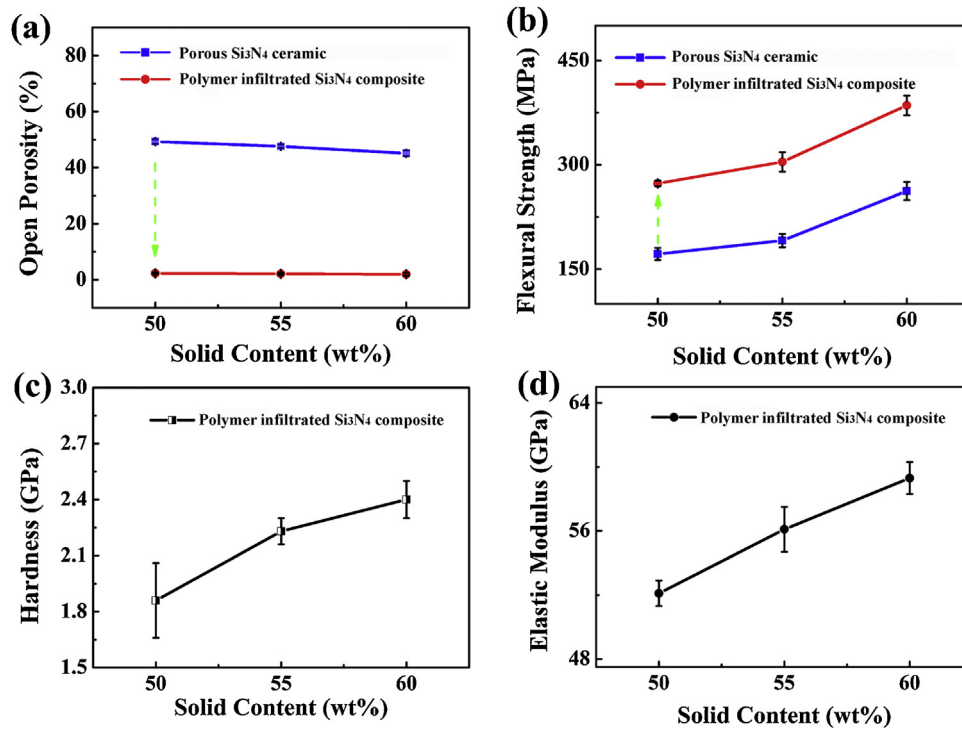


Fig. 2 – Physical and mechanical properties of porous Si<sub>3</sub>N<sub>4</sub> scaffolds and polymer infiltrated Si<sub>3</sub>N<sub>4</sub> composites as a function of solid content: (a) open porosity, (b) flexural strength, (c) hardness, (d) elastic modulus.

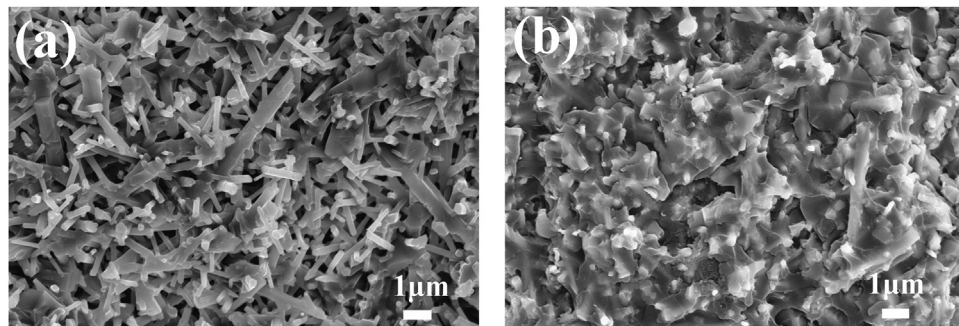


Fig. 3 – Micrographs of fracture surface from porous Si<sub>3</sub>N<sub>4</sub> ceramics SN50 (a) and polymer infiltrated Si<sub>3</sub>N<sub>4</sub> ceramics PSN50 (b).

porous scaffolds in polymer-infiltrated composites. Additionally, liquid-phase-sintered porous Si<sub>3</sub>N<sub>4</sub> ceramics possessed porous structure by clubbed grain stacking [19–22]. Excellent connectivity between these pores was ensured by this unique microstructure, which was important for fully infiltrating of polymer into pores. Thirdly, these elongated β-Si<sub>3</sub>N<sub>4</sub> grains could lead to cracks deflection in fracture, which would be beneficial to the mechanical performance of the composites [23,24]. In this work, porous Si<sub>3</sub>N<sub>4</sub> ceramics with moderate porosity and excellent mechanical strength were fabricated by gelcasting method as shown in Fig. 2. Porosity as well as flexural strength were able to be adjusted by controlling solid content of suspensions in preparing procedure. With increasing solid content of suspensions from 50 wt% to 60 wt%, open porosity of porous Si<sub>3</sub>N<sub>4</sub> ceramics decreased from 49.3% to 45.1%, while the flexural strength increased from 171.8 MPa to 262.3 MPa accordingly.

Polymer was infiltrated into porous Si<sub>3</sub>N<sub>4</sub> scaffolds to fabricate PISNCs. Fig. 2(a) indicated that pores in scaffolds were well filled by polymer, the porosity of PISNCs was lowered to 1.94%–2.28%. An impressive improvement in flexural strength after compositing was also detected from Fig. 2(b). The PSN60 possessed flexural strength of 385.3 ± 14.3 MPa, which was much higher than commercially resin-based composites [11] and comparable with Si<sub>3</sub>N<sub>4</sub>-bioglass composites [25]. The comparison of different polymer-based composites, including the result of present study was shown in Fig. 8. It was attractive to find out that the polymer infiltrated Si<sub>3</sub>N<sub>4</sub> composite showed super-high flexural strength. Generally, composites possessed flexural strength less than 200 MPa, had limited applications. Polymer infiltrated zirconia and silicon nitride ceramics could lead to composites with flexural strength higher than 300 MPa. Comparing to the polymer infiltrated zirconia composites with polymer content less than 30 vol%

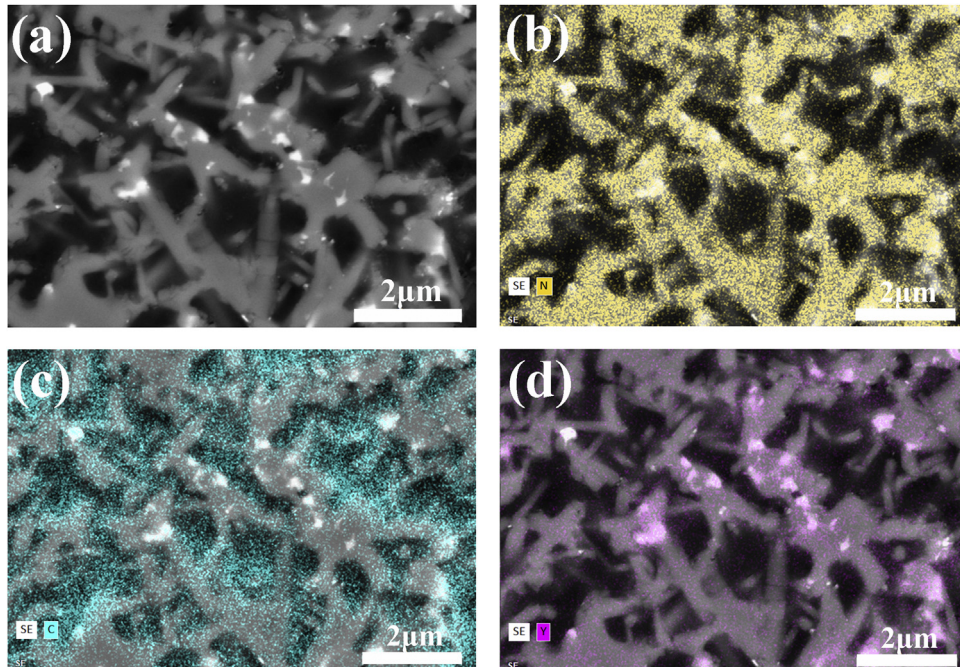


Fig. 4 – The back scattered electron (BSE) and corresponding energy dispersive spectrometer (EDS) images of polymer infiltrated  $\text{Si}_3\text{N}_4$  composite PSN50.

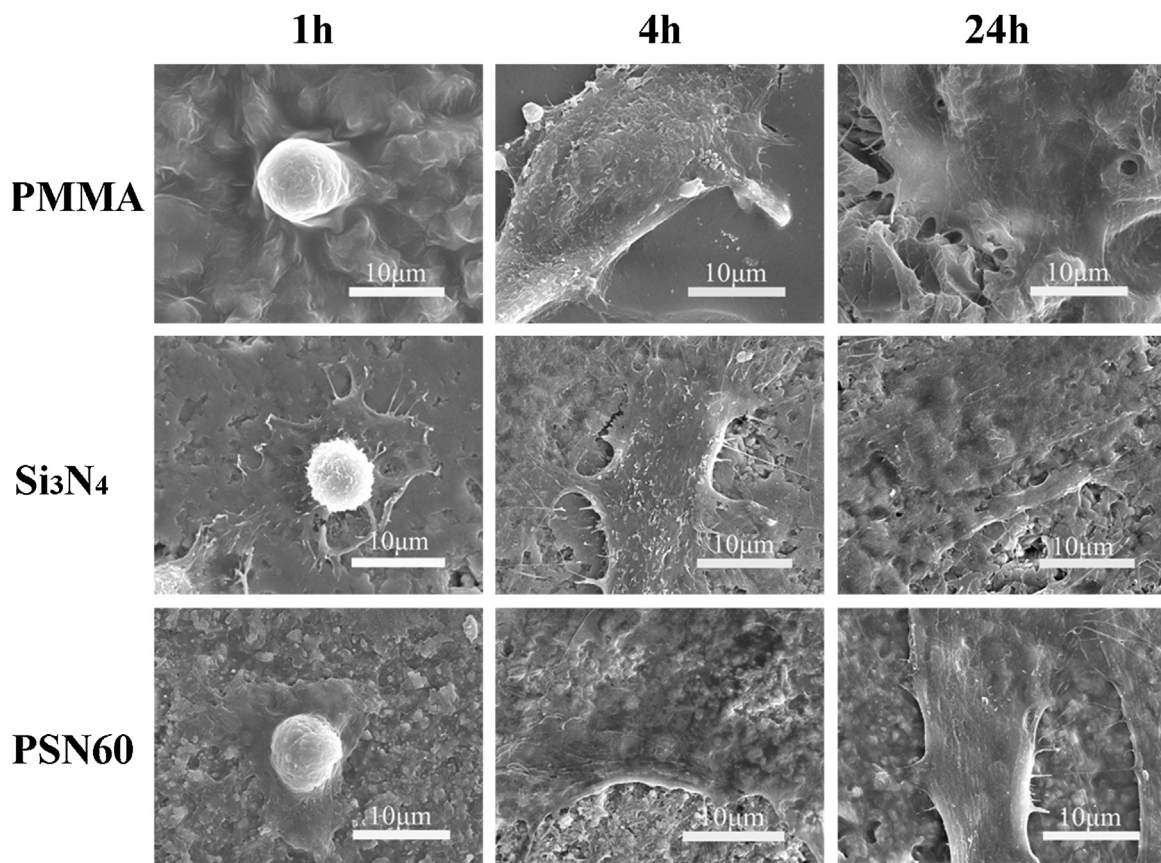


Fig. 5 – SEM morphologies of HGFs cultured on sample surfaces for various times.

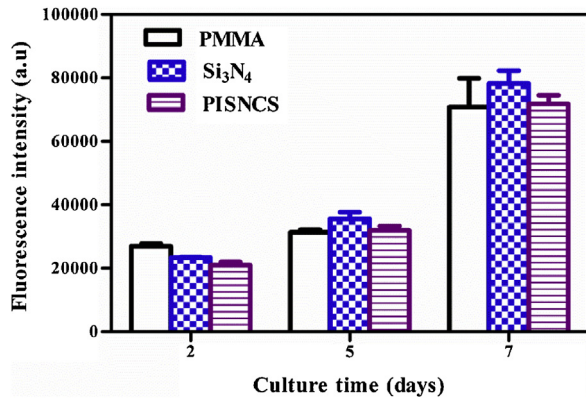


Fig. 6 – Fluorescence intensity of HGFs cultured on sample surfaces for various times.

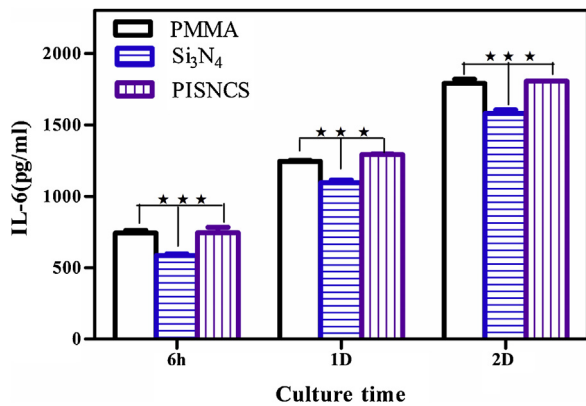


Fig. 7 – IL-6 release of HGFs cultured on sample surfaces for various times, \*\*\* $p < 0.001$ .

[29], the polymer content in PSN60 prepared in the present reached nearly up to 43 vol%, which could result in a better machinability.

Moreover, the hardness of PISNCs ranged from 1.86 GPa to 2.40 GPa, which were similar to the hardness of enamel [26]. Once referred to elastic modulus, more potential could be expected for PISNCs. It was believed that high modulus of ceramics might lead to stress shielding in body. While the elastic modulus of PISNCs (52.1–56.1 GPa) located closely to the modulus of cortical bone [25] and enamel [26], thus PISNCs could possess significant potentials in high load medical applications.

Micrographs of fracture surface from porous Si<sub>3</sub>N<sub>4</sub> ceramics SN50 showed uniform distribution of Si<sub>3</sub>N<sub>4</sub> grains and pores, which was important for the well mechanical performance of both porous scaffolds and PISNCs. These clubbed grains stacked together played essential roles in the high strength. After polymer infiltrating and curing, almost all pores were filled by polymer in Fig. 3b. However, several nanopores were still existed in the composites, these pores were originated from pores failed to be infiltrated or caused by resin shrinkage. The detail distribution of polymer and ceramic phases in the bicontinuous PISNC was shown in Fig. 4. Elements distribution in Fig. 4b–d of N, C, Y represented the

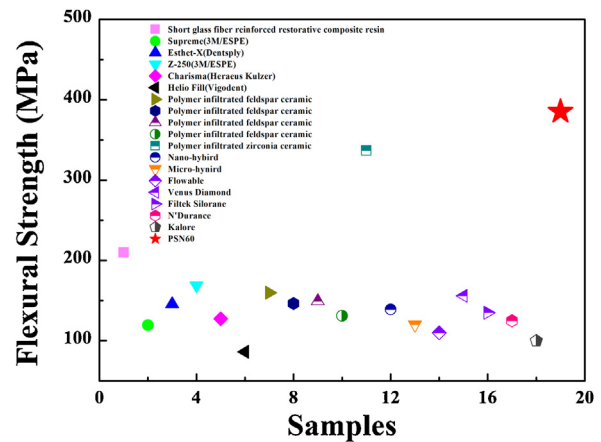


Fig. 8 – Flexural strength of various organic–inorganic composites [11,27,28,29,10]. The big red pentagram represents the flexural strength in this work. (For interpretation of the references to colour in this figure legend, the reader is referred to the web version of this article.)

distribution of Si<sub>3</sub>N<sub>4</sub>, PMMA and Y<sub>2</sub>O<sub>3</sub>, respectively, which agreed well with what was seen from BSE image in Fig. 4a. The connected pores in ceramic was filled by polymer phase, constructed a bicontinuous organic–inorganic composite.

Although high strength PMMA–Si<sub>3</sub>N<sub>4</sub> composites were obtained, it should be noted that some corner areas of pores formed by stacked grains in PISNCs were not fully infiltrated in this study, which might because the special pore structure caused by rod shape Si<sub>3</sub>N<sub>4</sub> grains. Thus the mechanical performance of PISNCs still had room for improvement. A schematic illustration of this phenomenon was shown in Fig. 9.

A schematic in Fig. 10 was used to explain this phenomenon through mechanical equilibrium. During the infiltrating, when polymer droplet infiltrated to the corner of stacked grains, a balance can be explained by the following equation:

$$F_i = F_p + 2\cos\theta F_f$$

Where,  $F_i$  is the force that pushing polymer forward,  $F_p$  is the force that caused by air left in the pores,  $F_f$  is the friction force between polymer and Si<sub>3</sub>N<sub>4</sub> grains. Under this mechanical balance, polymer cannot fill the pores completely and results in unfilled pores in PISNCs. If  $F_i$  had advantages over other forces, polymers would further infiltrating until a new balance was reached. In fact, as long as air remained in the pores, a balance would be reached anyhow since  $F_p$  increased along with volume compression. Thus, these pores were hard to be infiltrated completely in porous scaffolds. To achieve ideally infiltrated composites, vacuum treatment before and during infiltrating could be a good additional assistance, which would beneficial to the further improvement of the mechanical performance.

The cytocompatibility results showed that PSN60 possessed excellent performance on initial adhesion, spreading

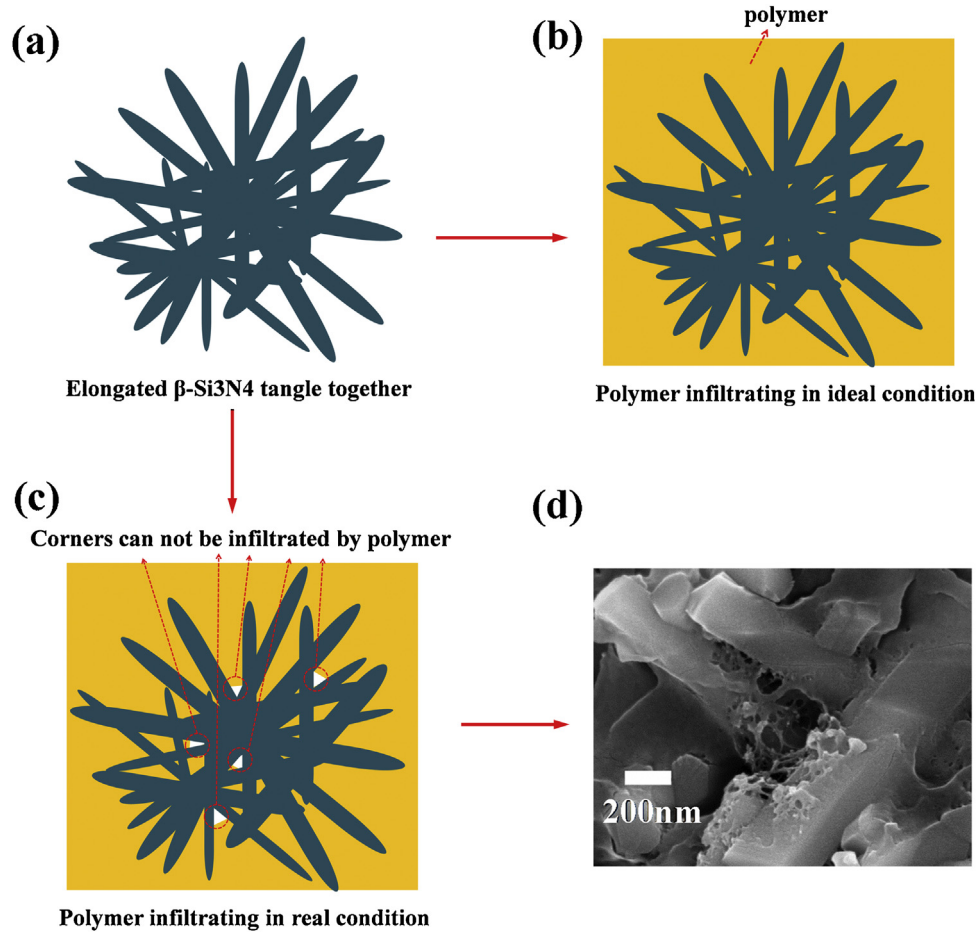


Fig. 9 – Schematic illustration of polymer infiltrating in porous  $\text{Si}_3\text{N}_4$  ceramics: (a)–(c). (d) shows corner area not fully infiltrated by polymer in the composite.

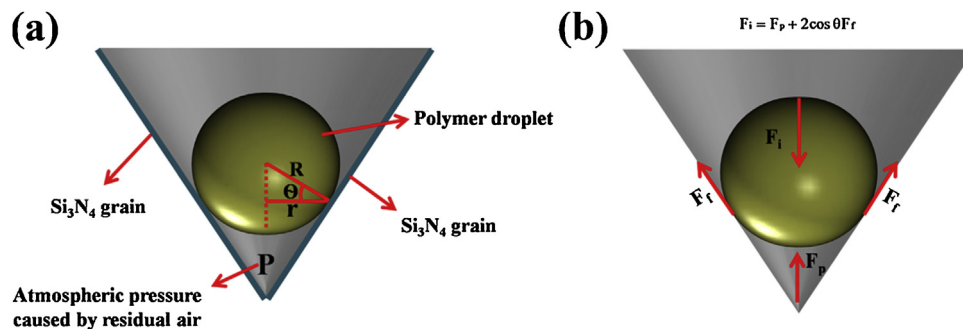


Fig. 10 – Schematic illustration of force equilibrium during polymer infiltration process in porous  $\text{Si}_3\text{N}_4$  ceramics at corner areas.

and proliferation of HGFs. IL-6 release behavior in HGFs cultured with materials was used to predict the early gingival and periodontal inflammation stimulated by three groups of materials. It showed that the three groups exhibited low IL-6 release implying that all the tested materials had slight inflammatory response. Since  $\text{Si}_3\text{N}_4$  ceramic is a stable bioinert material, it

showed a significantly lower level of IL-6 release than PMMA and PSN60 samples, indicating  $\text{Si}_3\text{N}_4$  ceramic had a superior biocompatibility. While, PSN60 showed a similar IL-6 release performance with PMMA. Since PMMA had been widely used in dental restorations, it indicated that PISNCs would be clinically safe.

## 5. Conclusions

In the present work, polymer-infiltrated  $\text{Si}_3\text{N}_4$  composites with excellent mechanical performance were fabricated from high strength porous  $\text{Si}_3\text{N}_4$  ceramics. PISNCs possessed excellent flexural strength with moderate hardness and elastic modulus. The flexural strength of PISNCs obtained from SN60 was high as 385.3 MPa, which contained a polymer volume nearly 43 vol%. Whereas, the hardness and elastic modulus of PSN60 were 2.4 GPa and 56.1 GPa, respectively, which were close to those of enamel. The excellent mechanical properties of PISNCs should be attributed to the special pore structure formed by elongated  $\text{Si}_3\text{N}_4$  grains and highly interconnected bicontinuous organic-inorganic microstructure. In addition, PISNCs also exhibited excellent biocompatibility on HGFs. PSN60 possessed excellent performance on initial adhesion, spreading and proliferation of HGFs, as well as a similar IL-6 release performance with PMMA. In conclusion, polymer-infiltrated  $\text{Si}_3\text{N}_4$  composites are mechanical promising candidates for dental restorations and high-load medical applications.

## Acknowledgments

This work was supported by Shanghai Committee of Science and Technology, China (17441904100).

## REFERENCES

- [1] FLR. Silicon nitride and related materials. *J Am Ceram Soc* 2000;83:245–65, <http://dx.doi.org/10.1111/j.1151-2916.2000.tb01182.xs>.
- [2] Jansen M. High performance non-oxide ceramics I. Springer Berlin Heidelberg; 2002, <http://dx.doi.org/10.1007/3-540-45613-9>.
- [3] Petzow G, Herrmann M. High performance non-oxide ceramics II. Springer Berlin Heidelberg; 2002, <http://dx.doi.org/10.1007/3-540-45623-6.2>.
- [4] Klemm Hagen. Silicon nitride for high-temperature applications. *J Am Ceram Soc* 2010;93:1501–22, <http://dx.doi.org/10.1111/j.1551-2916.2010.03839.x>.
- [5] Bodišová K, Kašiarová M, Domanická M, Hnatko M, Lenčič Z, Nováková ZV, et al. Porous silicon nitride ceramics designed for bone substitute applications. *Ceram Int* 2013;39:8355–62, <http://dx.doi.org/10.1016/j.ceramint.2013.04.015>.
- [6] Mazzocchi M, Bellosi A. On the possibility of silicon nitride as a ceramic for structural orthopaedic implants. Part I: processing, microstructure, mechanical properties, cytotoxicity. *J Mater Sci Mater Med* 2008;19:2881–7, <http://dx.doi.org/10.1007/s10856-008-3417-2>.
- [7] Mazzocchi M, Gardini D, Traverso PL, Faga MG, Bellosi A. On the possibility of silicon nitride as a ceramic for structural orthopaedic implants. Part II: chemical stability and wear resistance in body environment. *J Mater Sci Mater Med* 2008;19:2889–901, <http://dx.doi.org/10.1007/s10856-008-3437-y>.
- [8] Salgueiredo E, Vila M, Silva MA, Lopes MA, Santos JD, Costa FM, et al. Biocompatibility evaluation of DLC-coated  $\text{Si}_3\text{N}_4$  substrates for biomedical applications. *Diam Relat Mater* 2008;17:878–81, <http://dx.doi.org/10.1016/j.diamond.2007.08.019>.
- [9] Badran Z, Struillou X, Hughes FJ, Soueidan A, Hoornaert A, Ide M. Silicon nitride ( $\text{Si}_3\text{N}_4$ ) implants: the future of dental implantology? *J Oral Implantol* 2017;43:240–4, <http://dx.doi.org/10.1563/aaid-joi-D-16-00146>.
- [10] Ilie N, Hickel R. Resin composite restorative materials. *Aust Dent J* 2011;56(Suppl. 1):59–66, <http://dx.doi.org/10.1111/j.1834-7819.2010.01296.x>.
- [11] Rodrigues Junior SA, Zanchi CH, Carvalho RV, Demarco FF. Flexural strength and modulus of elasticity of different types of resin-based composites. *Braz Oral Res* 2007;21:16–21, <http://dx.doi.org/10.1590/S1806-83242007000100003>.
- [12] He LH, Swain M. A novel polymer infiltrated ceramic dental material. *Dent Mater* 2011;27:527–34, <http://dx.doi.org/10.1016/j.dental.2011.02.002>.
- [13] Wang F, Xiong Y, Ning C, Sun J, Zeng Y. Effects of pore connectivity and microstructure on mechanical performance of  $\text{ZrO}_2$  scaffolds and PMMA-infiltrated  $\text{ZrO}_2$  composites. *J Alloys Compd* 2017;728:189–95, <http://dx.doi.org/10.1016/j.jallcom.2017.08.277>.
- [14] Wang F, Gu H, Yin J, Yao D, Xia Y, Zuo K, et al. Porous  $\text{Si}_3\text{N}_4$  ceramics fabricated through a modified incomplete gelcasting and freeze-drying method. *Ceram Int* 2017;43:14678–82, <http://dx.doi.org/10.1016/j.ceramint.2017.07.194>.
- [15] Schmalz G, Schuster U, Schweikl H. Influence of metals on IL-6 release in vitro. *Biomaterials* 1998;19:1689–94, [http://dx.doi.org/10.1016/S0142-9612\(98\)00075-1](http://dx.doi.org/10.1016/S0142-9612(98)00075-1).
- [16] Young AC, Omatete OO, Janney MA, Menchhofer PA. Gelcasting of alumina. *J Am Ceram Soc* 1991;74:612–8, <http://dx.doi.org/10.1111/j.1151-2916.1991.tb04068.x>.
- [17] Omatete OO, Janney MA, Nunn SD. Gelcasting: from laboratory development toward industrial production. *J Eur Ceram Soc* 1997;17:407–13, [http://dx.doi.org/10.1016/S0955-2219\(96\)00147-1](http://dx.doi.org/10.1016/S0955-2219(96)00147-1).
- [18] Wang F, Gu H, Yin J, Xia Y, Zuo K, Liang H, et al. Porous  $\text{Si}_3\text{N}_4$  fabrication via volume-controlled foaming and their sound absorption properties. *J Alloys Compd* 2017;727:163–7, <http://dx.doi.org/10.1016/j.jallcom.2017.07.232>.
- [19] Li X, Zhang L, Yin X. Effect of chemical vapor infiltration of  $\text{Si}_3\text{N}_4$  on the mechanical and dielectric properties of porous  $\text{Si}_3\text{N}_4$  ceramic fabricated by a technique combining 3-D printing and pressureless sintering. *Scr Mater* 2012;67:380–3, <http://dx.doi.org/10.1016/j.scriptamat.2012.05.030>.
- [20] Yang JF, Deng ZY, Ohji T. Fabrication and characterisation of porous silicon nitride ceramics using  $\text{Yb}_2\text{O}_3$  as sintering additive. *J Eur Ceram Soc* 2003;23:371–8, [http://dx.doi.org/10.1016/S0955-2219\(02\)00175-9](http://dx.doi.org/10.1016/S0955-2219(02)00175-9).
- [21] Li X, Wu P, Zhu D. Effect of foaming pressure on the properties of porous  $\text{Si}_3\text{N}_4$  ceramic fabricated by a technique combining foaming and pressureless sintering. *Scr Mater* 2013;68:877–80, <http://dx.doi.org/10.1016/j.scriptamat.2013.02.033>.
- [22] Wang F, Yin J, Yao D, Xia Y, Zuo K, Liang H, et al. Effects of oil on gelcasting of oil-in-water  $\text{Si}_3\text{N}_4$  suspensions. *J Alloys Compd* 2016;699:268–73, <http://dx.doi.org/10.1016/j.jallcom.2016.12.377>.
- [23] Lu LM, Zuo KH, Zeng YP. Fabrication and properties of surface-modified  $\beta\text{-Si}_3\text{N}_4$  whiskers reinforced dental resin composites. *J Appl Polym Sci* 2013;128:41–6, <http://dx.doi.org/10.1002/app.38125>.
- [24] Bal BS, Rahaman MN. Orthopedic applications of silicon nitride ceramics. *Acta Biomater* 2012;8:2889, <http://dx.doi.org/10.1016/j.actbio.2012.04.031>.
- [25] Amaral M, Lopes MA, Silva RF, Santos JD. Densification route and mechanical properties of  $\text{Si}_3\text{N}_4$ -bioglass biocomposites. *Biomaterials* 2002;23:857, [http://dx.doi.org/10.1016/S0142-9612\(01\)00194-6](http://dx.doi.org/10.1016/S0142-9612(01)00194-6).

- [26] Cuy JL, Mann AB, Livi KJ, Teaford MF, Weihs TP. Nanoindentation mapping of the mechanical properties of human molar tooth enamel. *Arch Oral Biol* 2002;47:281–91, [http://dx.doi.org/10.1016/S0003-9969\(02\)00006-7](http://dx.doi.org/10.1016/S0003-9969(02)00006-7).
- [27] Garoushi S, Vallittu PK, Lassila LV. Short glass fiber reinforced restorative composite resin with semi-inter penetrating polymer network matrix. *Dent Mater* 2007;23:1356–62, <http://dx.doi.org/10.1016/j.dental.2006.11.017>.
- [28] Coldea A, Swain MV, Thiel N. Mechanical properties of polymer-infiltrated-ceramic-network materials. *Dent Mater* 2013;29:419–26, <http://dx.doi.org/10.1016/j.dental.2013.01.002>.
- [29] Li J, Cui BC, Lin YH, Deng XL, Li M, Nan CW. High strength and toughness in chromatic polymer-infiltrated zirconia ceramics. *Dent Mater* 2016;32:1555–63, <http://dx.doi.org/10.1016/j.dental.2016.09.003>.